Electronic and magnetic properties of nanographite ribbons

Katsunori Wakabayashi
Yukawa Institute for Theoretical Physics, Kyoto University, Kyoto 606-8502, Japan and Institute of Materials Science, University of Tsukuba, Tsukuba 305-8573, Japan

Mitsutaka Fujita*
Institute of Materials Science, University of Tsukuba, Tsukuba 305-8573, Japan

Hiroshi Ajiki
Department of Material Physics, Osaka University, Osaka 560-8531, Japan

Manfred Sigrist
Yukawa Institute for Theoretical Physics, Kyoto University, Kyoto 606-8502, Japan
(Received 18 September 1998)

Electronic and magnetic properties of ribbon-shaped nanographite systems with zigzag and armchair edges in a magnetic field are investigated by using a tight-binding model. One of the most remarkable features of these systems is the appearance of edge states, strongly localized near zigzag edges. The edge state in a magnetic field, generating a rational fraction of the magnetic flux ($\phi = p/q$) in each hexagonal plaquette of the graphite plane, behaves like a zero-field edge state with q internal degrees of freedom. The orbital diamagnetic susceptibility strongly depends on the edge shapes. The reason is found in the analysis of the ring currents, which are very sensitive to the lattice topology near the edge. Moreover, the orbital diamagnetic susceptibility is scaled as a function of the temperature, Fermi energy, and ribbon width. Because the edge states lead to a sharp peak in the density of states at the Fermi level, the graphite ribbons with zigzag edges show Curie-like temperature dependence of the Pauli paramagnetic susceptibility. Hence, there is a crossover from high-temperature diamagnetic to low-temperature paramagnetic behavior in the magnetic susceptibility of nanographite ribbons with zigzag edges. [S0163-1829(99)02111-6]

I. INTRODUCTION

Nanographites are nanometer-sized graphite fragments that represent a new class of a mesoscopic system intermediate between aromatic molecules and extended graphite sheets. In these systems the boundary regions play an important role so that edge effects may influence strongly the π-electron states near the Fermi energy. A useful and simple system to investigate the electronic states of nanographites is provided by ribbon-shaped graphite sheets. The study of the electronic states of graphite ribbons based on the tight-binding model reveals that the edge shape — we distinguish between *zigzag* and *armchair* edges (see Fig. 1) — leads to strikingly different properties of the states near the Fermi level. The ribbons with zigzag edges possess partly flat bands at the Fermi level corresponding to electronic states localized in the near vicinity of the edge. These localized states (''edge states'') correspond to the nonbonding molecular orbital (NBMO) as can be seen examining the analytic solution for semi-infinite graphite with a zigzag edge.[1,2] In contrast, localized edge states and the corresponding flat bands are completely absent for ribbons with armchair edges.

The localized edge states are of special interest in nanographite physics, because of their relatively large contribution to the density of states (DOS) at the Fermi energy. There is a tendency towards a Fermi surface instability that is important to examine. Previously, it was reported that based on the Su-Schrieffer-Hegger model the electron-phonon interaction does not induce a lattice distortion because of the nonbonding character of the edge states.[3] On the other hand, the electron-electron interaction on the level of an unrestricted Hartree-Fock approximation (HFA) yields a ferrimagnetic spin polarization at the zigzag edges and an energy gap at the Fermi level.[1,4] The effect of long-range Coulomb interaction on the edge state was examined using the Par-Parier-Pople model with the restricted HFA which does not allow any spin polarization. The conclusion was that long-range Coulomb interaction does not destroy the edge state as well as the flat bands.[5] This result was further confirmed by first principle calculations based on local density approximation.[6]

The stability of the edge states has been extensively investigated from various points of view. One remaining problem is the influence of an external magnetic field. How are the edge states affected? Is their NBMO character preserved? The answers to these questions will be important for future studies of the electronic, magnetic, and transport properties of nanographites. For this purpose we investigate here the magnetic properties, especially magnetic susceptibility, for the case of noninteracting electrons.

The observed magnetic susceptibility χ is the sum of four components: (1) localized spin susceptibility χ_{spin}, (2) diamagnetic susceptibility due to the core electrons χ_{core}, (3) Pauli paramagnetic susceptibility χ_P, and (4) orbital diamagnetic susceptibility $\chi_{orb,}$ due to the cyclotron motion of the itinerant electrons.

Since we neglect electron-electron interaction throughout

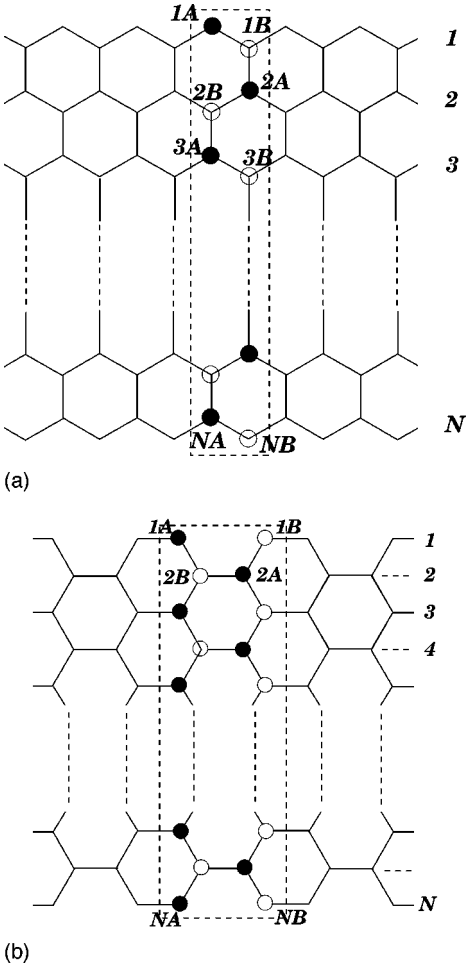

FIG. 1. The structure of graphite ribbons with (a) zigzag edges and (b) armchair edges. The rectangle with the dashed line is the unit cell.

this paper, χ_{spin} can be neglected. Furthermore, χ_{core} is unimportant for us, because it is small and basically temperature independent. On the other hand, the Pauli paramagnetic susceptibility is related to the DOS at the Fermi level, which represents an important component in zigzag nanographite ribbons where an enhanced density of states appears at the Fermi level. Note that χ_P is negligible in armchair ribbons, aromatic molecules, and graphite sheets, because their DOS is suppressed at the Fermi level. We will see below that the fact that the DOS introduced by the edge states is sharply peaked at the Fermi energy, χ_P introduces a very pronounced temperature dependence, which is nearly Curie-like. The diamagnetic contribution to the susceptibility is very familiar from the magnetic properties of graphite sheets. It is due to the orbital cyclotron motion of the electrons in a field with a finite component perpendicular to the plane. Naturally, this diamagnetic response is very anisotropic and only weakly temperature dependent. From this we can conclude that in nanographite ribbons with zigzag edges the susceptibility should consist mainly of these two competing contributions χ_P and $\chi_{orb.}$. Hence, a crossover occurs from a high-temperature diamagnetic to a low-temperature paramagnetic regime, where the characteristic temperature depends on the width of the ribbon and of the orientation of the external field. It is worth noting that the field direction is an important tool to distinguish the magnitude of the two components.

II. ELECTRONIC STRUCTURE OF GRAPHITE RIBBONS IN MAGNETIC FIELD

A. Harper equation

In this paper, we use a single-orbital nearest-neighbor tight-binding model in order to study the electronic states of nanographite ribbons. This model has been successfully used for the calculation of electronic states of fullerene molecules, carbon nanotubes, and other carbon-related materials.[7,8] The Hamiltonian is written as

$$H=\sum_{\langle i,j\rangle} t_{ij}c_i^{\dagger}c_j, \tag{2.1}$$

where the operator $c_i^{\dagger}$ creates an electron on the site i, $\langle i,j\rangle$ denotes the summation over the nearest-neighbor sites. Here, we neglect spin indices for simplicity. In this model, the magnetic field $\boldsymbol{B}$ perpendicular to the graphite plane is incorporated in the transfer integral t_{ij} by means of the Peierls phase,[9] defined as

$$t_{ij}\rightarrow t_{ij}\mathrm{e}^{\mathrm{i}2\pi\phi_{i,j}}, \tag{2.2}$$

where $\phi_{i,j}$ is given by the line integral of the vector potential from i site to j site,

$$\phi_{i,j}=\frac{e}{ch}\int_i^j \mathrm{d}\boldsymbol{l}\cdot\boldsymbol{A}. \tag{2.3}$$

The magnetic flux through the area S in units of the flux quantum $\phi_o=ch/e$ is

$$\frac{1}{\phi_0}\int \mathrm{d}\mathbf{S}\cdot\mathbf{B}=\frac{e}{ch}\oint \mathrm{d}l\cdot A=\sum_{around\mathbf{S}}\phi_{i,j}. \tag{2.4}$$

The structure of graphite ribbons with zigzag and armchair edges are shown in Fig. 1, where we assume that all edge sites are terminated by hydrogen atoms. The ribbon width N is defined by the number of zigzag lines for the zigzag ribbon and by the number of dimer lines for the armchair ribbons. Since a hexagonal lattice can be divided by two sublattices, we call the A(B)-sublattice on the nth zigzag or dimer line as the nA (nB) site. We assume Landau gauge with $\boldsymbol{A}=(0,\mathrm{Bx},0)$, where we define the translational invariant direction of each ribbon as the y axis, and the x axis lies perpendicular to y axis. In this gauge, the unit cell of each ribbon could be taken as the rectangle shown in Fig. 1.

It should be noted that the same number N for both zigzag and armchair ribbons does not give the same ribbon width, when the ribbons are measured by the same unit of length. Therefore, when we compare physical quantities of zigzag and armchair ribbons with a same width W, we will use the following definition:

$$W=\begin{cases}\dfrac{\sqrt{3}}{2}Na-a\equiv W_z & \text{zigzag ribbons}\\[2ex] (N-1)\dfrac{\sqrt{3}}{2}a\equiv W_a & \text{armchair ribbons,}\end{cases} \tag{2.5}$$

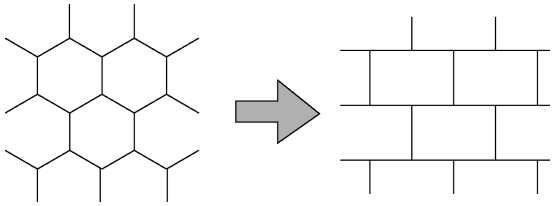

FIG. 2. The transformation from hexagonal lattice to brick-type lattice, which does not change the lattice topology.

where a is the C-C bond length.

Next, let us apply Eq. (2.1) to the graphite lattice and derive the so-called Harper equations. In order to apply Eq. (2.1) to the graphite lattice and simplify the formulation, we introduce the lattice transformation as shown in Fig. 2, which does not change the lattice topology. For convenience we will use this brick-type lattice structure whenever we perform real calculations.

The Peierls phase for the graphite ribbons is easily calculated from Eq. (2.3). The Peierls phase of graphite ribbons with (a) zigzag and (b) armchair ribbons is shown in Fig. 3. For both cases, the Peierls phase is given by $\phi_{mB,nA}=1/2m\phi\delta_{mn}$, where ϕ is the magnetic flux through a plaquette in units of a quantum flux.

Now, let us derive the Harper equation, which possess the translational symmetry along the zigzag axis. In order to apply Eq. (2.1) to zigzag ribbons, we define a new operator $c_\alpha(i)$, which creates an electron on the site i in the unit cell α. The momentum representation of this operator in the y direction is defined by

$$c_\alpha(i)=\frac{1}{\sqrt{L}}\sum_k \mathrm{e}^{\mathrm{i}kr_\alpha}\gamma_k(i), \tag{2.6}$$

where r_α represents the position of the unit cell α. Here we also define a one-particle state

$$|\Psi(k)\rangle=\sum_m [\Psi_{mA}(k)\gamma^\dagger_{mA}(k)+\Psi_{mB}(k)\gamma^\dagger_{mB}(k)]|0\rangle. \tag{2.7}$$

Inserting this one-particle state into the Schrödinger equation $H|\Psi\rangle=\epsilon|\Psi\rangle$, we can easily obtain the following four eigenvalue equations for the sites mB, mA, and $(m+1)A$,

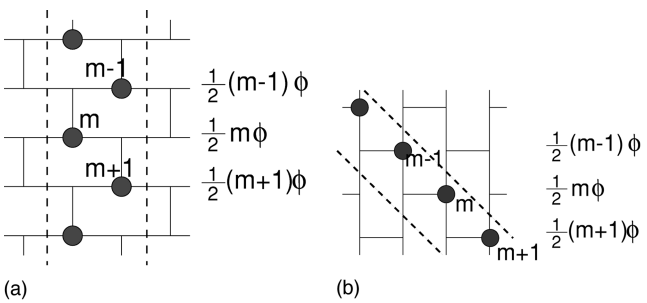

FIG. 3. The Peierls phase for Landau gauge on (a) zigzag ribbons and (b) armchair ribbons.

$$\begin{aligned}\epsilon\Psi_{mB}&=\Psi_{(m+1)A}+\mathrm{e}^{\mathrm{i}2\pi(m/2)\phi}\Psi_{mA}+\mathrm{e}^{-\mathrm{i}2\pi(m/2)\phi}\Psi_{mA},\\ \epsilon\Psi_{mA}&=\Psi_{(m-1)B}+\mathrm{e}^{\mathrm{i}2\pi(m/2)\phi}\Psi_{mB}+\mathrm{e}^{-\mathrm{i}2\pi(m/2)\phi}\Psi_{mB},\\ \epsilon\Psi_{(m+1)A}&=\Psi_{mB}+\mathrm{e}^{\mathrm{i}2\pi(m/2)\phi}\Psi_{(m+1)B}+\mathrm{e}^{-\mathrm{i}2\pi(m/2)\phi}\Psi_{(m+1)B}.\end{aligned} \tag{2.8}$$

Eliminating the A-sublattice sites, we obtain the difference equation,

$$\lambda\Psi_m(k_y)=a_m\Psi_{m+1}(k_y)+b_m\Psi_m(k_y)+a_{m-1}\Psi_{m-1}(k_y), \tag{2.9}$$

where $\lambda=\epsilon^2-3$, $a_m(k_y)=2\cos(k_y/2+m\pi\phi)$, $b_m(k_y)=2\cos(k_y+2m\pi\phi)$, and Ψ_{mB} was replaced by Ψ_m. Therefore, our problem was reduced to a one-dimensional tight- binding model with a superlattice potential of period $2q$ for a rational flux $\phi=p/q$. Note that this equation does not include any boundary conditions yet. It may be applied to both graphite ribbons and sheets by imposing the appropriate boundary conditions. In the following calculations, the factor $m\pi\phi$ will be replaced by $[(N-1)/2-m+1]\pi\phi$ to keep the energy band symmetric about $k=0$ for arbitrary magnetic flux. This replacement means that the origin of the x axis is set to the center of the ribbons.

The spectrum is confined to values of λ between -6 and $+6$, i.e., $-3\leqslant\epsilon\leqslant+3$. A close inspection shows that the following translations do not change the energy spectrum; $\epsilon\rightarrow-\epsilon$ and $\phi\rightarrow\phi+n$, where n is an arbitrary integer. For rational flux $\phi=p/q$, a_m is a function with period $2q$ and b_m is a function with period q. In addition, we must pay attention to the following symmetry of the energy bands in the Brillouin zone,

$$\epsilon\left(k_y+\frac{2\pi}{q}n\right)=\epsilon(k_y). \tag{2.10}$$

Here we should again note that these arguments do not depend on the boundary conditions.

Similarly, we can also derive the Harper equations, which includes the translational symmetry along the armchair axis. In the same way as Eq. (2.9), the following equation is obtained,

$$\begin{aligned}\lambda\Psi_m(k_y)=&\Psi_{m+2}(k_y)+a_m\Psi_{m+1}(k_y)\\&+a_m\Psi_{m-1}(k_y)+\Psi_{m-2}(k_y),\end{aligned} \tag{2.11}$$

where

$$\lambda=\epsilon^2-3,\ a_m(k_y)=2\cos[k_y/2+(m-1/2)\pi\phi]\mathrm{e}^{-\mathrm{i}(\pi/2)\phi}.$$

It is easy to confirm that the same symmetry properties as for Eq. (2.9) apply here too. Similarly, the factor a_m will be replaced by $a_m(k_y)=2\cos\{k_y/2+[(N-1)/2-2m+3]\pi\phi\}\mathrm{e}^{-\mathrm{i}\pi\phi}$ in order to obtain the symmetric energy band structure about $k=0$ for arbitrary magnetic flux.

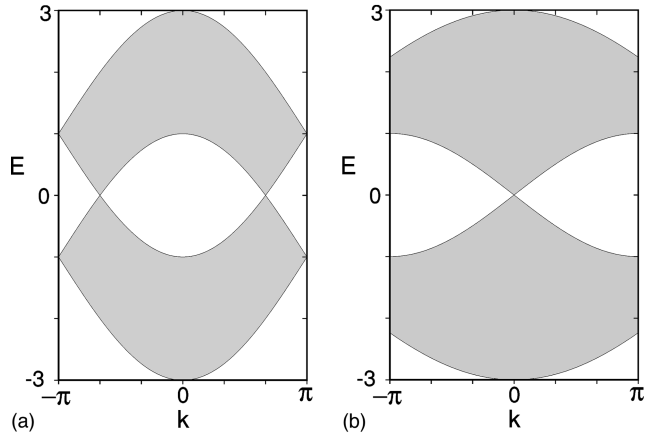

FIG. 4. The energy band structure of graphite sheet projected to (a) zigzag axis and (b) armchair axis in the absence of the magnetic field.

B. Graphite sheet

In this subsection, we consider the electronic structures of a graphite sheet in a magnetic field. This will afterwards become the basis to discuss the electronic structures of nanographite ribbons. As we have seen in the previous subsection, the tight-binding model of the graphite lattice could be reduced to a tight-binding model with superlattice potential of period $2q$. In order to calculate the energy spectrum of the graphite sheet, we must treat the eigenvalue problem of a $2q\times 2q$ matrix with the periodic-boundary condition $\Psi_{2q+1}=e^{ik_x 2q}\Psi_1$, when the Brillouin zone is reduced to the magnetic Brillouin zone $-\pi/2q\leqslant k_x\leqslant\pi/2q$ and $-\pi\leqslant k_y\leqslant\pi$.

At the beginning, we consider the zero-field energy band of the graphite sheet. By setting $\phi=0$ in Eqs. (2.9) and (2.11), the zero-field spectrum is easily obtained. From Eq. (2.9), we find for the graphite sheet with translational symmetry along the zigzag axis,

$$\epsilon_{\boldsymbol{k}}=\pm\sqrt{3+2\cos(k_y)+4\cos\left(\frac{k_y}{2}\right)\cos(k_x)}. \quad (2.12)$$

Similarly, from Eq. (2.11), the zero-field spectrum of graphites with translational symmetry along the armchair axis is

$$\epsilon_{\boldsymbol{k}}=\pm\sqrt{3+2\cos(2k_x)+4\cos\left(\frac{k_y}{2}\right)\cos(k_x)}. \quad (2.13)$$

The energy band structures for both Eqs. (2.12) and (2.13) are shown in Fig. 4, where k_y is replaced by k and we have superposed all k_x values in the spectrum. We can find the degeneracy at $\epsilon=0$ in both figures, which originates from the *K*-point degeneracy of the band structure of the graphite sheet.[1,2]

The spectrum of the graphite sheet in a magnetic field is shown in Fig. 5, which was first calculated by Rammal[15]. We can easily find that the spectrum has the fine recursive structure of the Hofstadter butterfly.[13] In the weak-magnetic-field limit, we can clearly see the Landau levels. When the magnetic flux is getting larger, these levels form the Landau subbands because of the Harper broadening. As we pointed out in the previous subsection, for the rational flux $\phi=p/q$, we can see $2q$ subbands with a reflection symmetry about $\epsilon=0$ and about $\phi=1/2$. Interestingly, the degeneracy at $\epsilon=0$ exits for arbitrary flux, which confirms that the *K*-point degeneracy will not be destroyed.

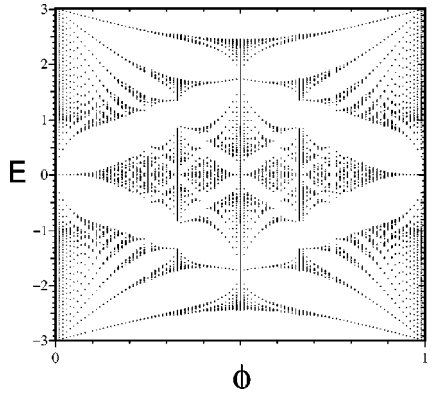

FIG. 5. The energy spectrum of the graphite sheet in a magnetic field.

As an example of the energy band structure in a strong magnetic field, we show the case of the graphite sheet projected to the (a) zigzag axis and (b) armchair axis for $\phi=1/4$ (Fig. 6). In a strong magnetic field, the Landau levels change to 2×4 subbands due to Harper broadening and the effect of the lattice structure gets more important, so that each subband has the basic structure of the zero-field case. Furthermore, we find the symmetry $\epsilon[k_y+(2\pi/q)n]=\epsilon(k_y)$.

C. Graphite ribbon

The energy band structures of graphite ribbons are obtained in terms of the Harper equation by imposing open boundary conditions. In the case of zigzag ribbons with width *N*, the boundary condition is $\Psi_{N+1}=\Psi_0=0$. However, we need a more careful treatment of the Harper equation at the edge site. In Eqs. (2.9), it was not considered that

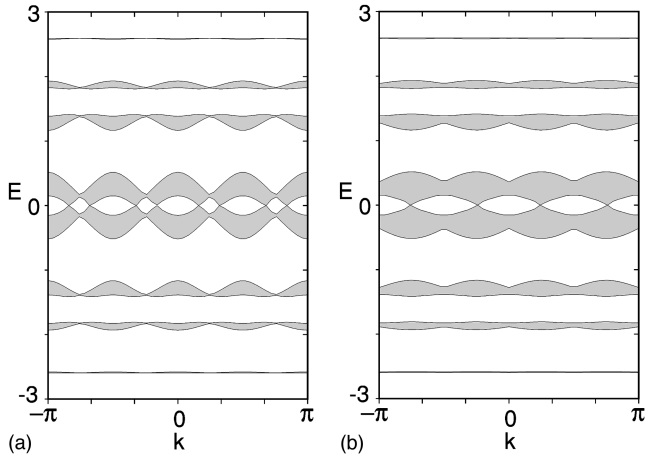

FIG. 6. The energy band structure of the graphite sheet projected to (a) zigzag axis and (b) armchair axis for $\phi=1/4$.

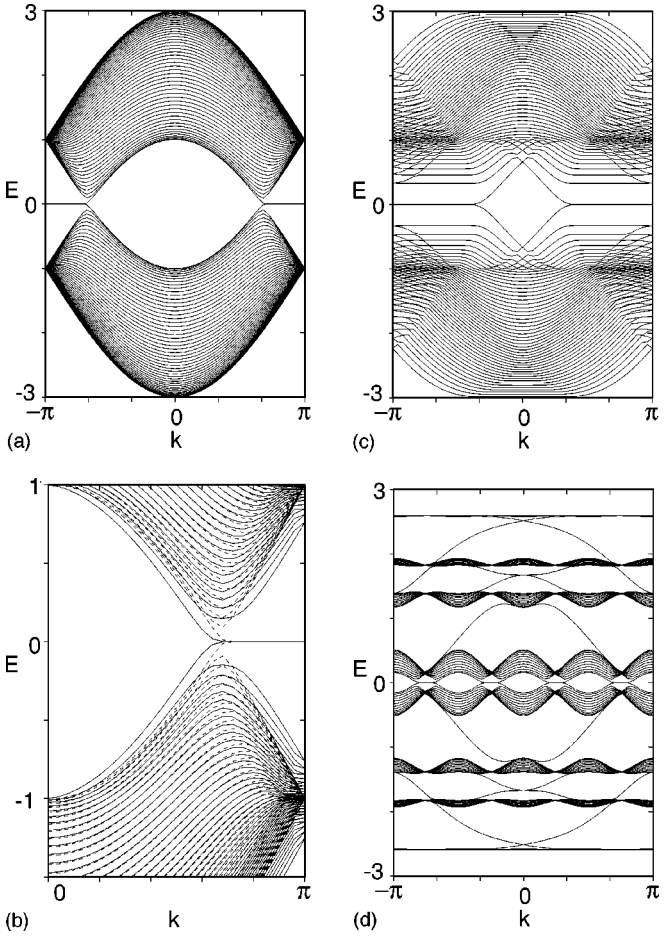

FIG. 7. The energy band structures of zigzag ribbon with $N=50$ for (a) $\phi=0$, (b) $\phi=1/500$, (c) $\phi=1/100$, and (d) $\phi=1/4$ for $\phi=1/4$. The dashed line in (b) is the energy structure at $\phi=0$ for comparison.

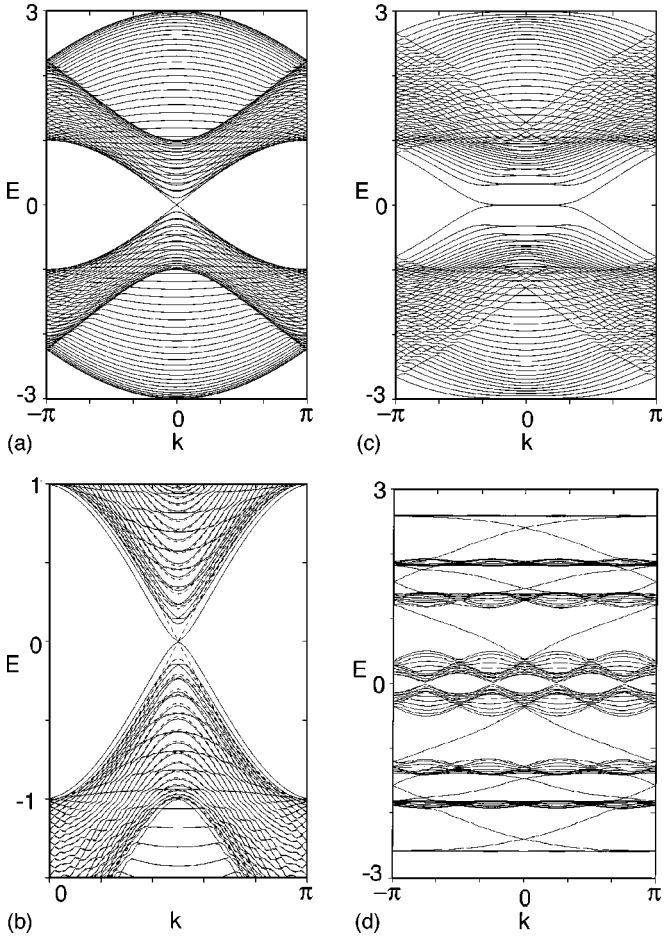

FIG. 8. The energy band structures of armchair ribbon with $N=50$ for (a) $\phi=0$, (b) $\phi=1/500$, (c) $\phi=1/100$, and (d) $\phi=1/4$ for $\phi=1/4$. The dashed line in (b) is the energy structure at $\phi=0$ for comparison.

there would be no $0A(B)$ and $(N+1)A(B)$ site. Including this fact, only for $m=1$ and N, the Eq. (2.9) has to be rewritten as

$$\lambda\Psi_m(k_y)=a_m\Psi_{m+1}(k_y) + (b_m-1)\Psi_m(k_y)=+a_{m-1}\Psi_{m-1}(k_y). \tag{2.14}$$

Therefore, we must replace $b_1(b_N)$ by $b_1-1(b_N-1)$ in Eq. (2.9) in order to include the condition that the $0A$ and $(N+1)A$ sites do not exist. Similarly, for the armchair ribbons, the boundary condition is $\Psi_{N+1}=\Psi_0=0$, where we must replace $b_1(b_N)$ by $b_1-1(b_N-1)$ in order to include the condition that the $0A$ and $(N+1)A$ sites do not exist.

We show the energy band structures of the zigzag ribbon with $N=50$ for $\phi=0,1/500,1/100,1/4$ in Figs. 7(a)—7(d). For $\phi=0$, the profile of band structure has almost the same structure as in the case of the graphite sheet as shown in Fig. 4(a). However, we can see partly flat bands at $E=0$, which do not appear in the energy band of the graphite sheet. The electronic states corresponding to partly flat bands are the strongly localized states near the zigzag edges, called ''edge states.'' Analytical properties will be discussed in the next section.

In the case of $q\geqslant N$, the Landau levels are not perfectly formed and the band structure at $\phi=0$ is almost unchanged, because the edges interrupt the cyclotron motion of the electron [Fig. 7 (b)]. For $q\leqslant N$, where the ribbon width is sufficiently wide compared with the cyclotron radius, the Landau levels are nearly developed [Fig. 7 (c)].

As an example for $q\ll N$ and higher commensurates, we show the energy band structure of $\phi=1/4$ in Fig. 7(d). The 2×4 Landau subbands are formed. Between the Landau subbands, we can see the additional dispersion. The states of these dispersions are also localized at the edge,[10,14,16] which originate from the cyclotron motion of electrons and not for topological reason. It should be noted that the partly flat bands are formed at $E=0$ again.

Next, we show the energy band structures of the armchair ribbon with $N=50$ for $\phi=0,1/500,1/100,1/4$ in Figs. 8(a)—8(d). For $\phi=0$, the profile of the band structure is almost identical to the one of the graphite sheet [Fig. 5 (a)]. Here, we cannot see partly flat bands at $E=0$.

In the case of $q\geqslant N$, the Landau levels are not perfectly formed and the band structure at $\phi=0$ does not change. For $q\leqslant N$, where the ribbon width is sufficiently wide compared with the cyclotron radius, the Landau levels are again almost formed as shown in Fig. 8. For the case of $q\ll N$ and higher commensurate fluxes, we show the energy bands structure of

$\phi = 1/4$ in Fig. 8(d). We also find that despite the additional dispersion between Landau subbands, no partly flat bands, as may occur in zigzag ribbons, are present at $E=0$ even in a magnetic field.

III. EDGE STATE

The states corresponding to the partly flat bands are analytically derived by Fujita and co-workers for the semi-infinite graphite sheet with a zigzag edge.[1,2] It can be understood as localized states near the zigzag edge. It is also possible to find the edge states by solving the Harper Eq. (2.9).

At the beginning, let us rewrite the Eq. (2.9) to the transfer matrix form,

$$\begin{pmatrix} \Psi_{m+1} \\ \Psi_m \end{pmatrix} = \begin{pmatrix} \frac{1}{a_m}(\lambda - \tilde{b}_m) & \frac{a_{m-1}}{a_m} \\ 1 & 0 \end{pmatrix} \begin{pmatrix} \Psi_m \\ \Psi_{m-1} \end{pmatrix}, \quad (3.1)$$

where $\tilde{b}_m$ is $b_m - 1$ for $m=1$, N and b_m for others. Let us take open boundary conditions, i.e,

$$\begin{pmatrix} \Psi_1 \\ \Psi_0 \end{pmatrix} = \begin{pmatrix} 1 \\ 0 \end{pmatrix} \quad (3.2)$$

and we impose the condition $\epsilon = 0$. One can obtain,

$$\Psi_n = D_k^{n-1}, \quad (3.3)$$

where D_k is $-2\cos(\frac{k}{2})$. Then the convergence condition $|D_k| \leqslant 1$ is required, because otherwise the wave function would diverge in the semi-infinite graphite sheet. This convergence condition defines the region $2\pi/3 \leqslant k \leqslant \pi$, where the partly flat bands exist. The charge density is shown in Fig. 9 at (a) $k=\pi$, (b) $8\pi/9$, (c) $7\pi/9$, and (d) $2\pi/3$. At $k=\pi$, the charge is perfectly localized at the zigzag edge. When the wave number deviates from $k=\pi$, the electron gradually penetrates towards the inner sites. Finally, the electron states completely extend at $k=2\pi/3$.

Similarly, the case of finite magnetic field, using Eqs. (3.1) and (3.2) under the condition of $\epsilon = 0$, we can derive the wave function on the nth zigzag line as

$$\Psi_n = \Pi_{i=1}^{n} D_k(i), \quad (3.4)$$

where

$$D_k(i) = \begin{cases} -2\cos\left(\frac{k}{2} - \frac{N-2i+1}{2}\pi\phi\right) & (i \geqslant 2) \\ 1 & (i=1). \end{cases} \quad (3.5)$$

For the rational flux $\phi = p/q$, there is a relation of $D_k(i+q) = D_k(i)$, so that in the case of semi-infinite graphite Eq. (3.4) might be rewritten as

$$\Psi_{nq} = (\Delta_k)^{n-1}, \quad (3.6)$$

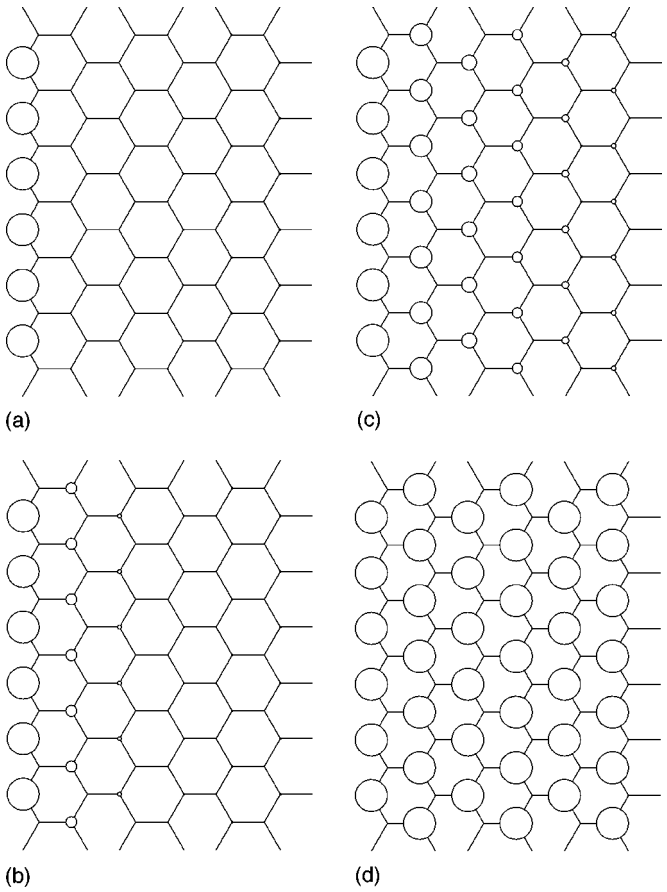

FIG. 9. The charge density of the edge state at (a) $k=\pi$, (b) $k=8\pi/9$, (c) $k=7\pi/9$, and (d) $k=2\pi/3$, where the radius of the circle means the magnitude of the charge density.

where

$$\Delta_k = \Pi_{i=1}^{q} D_k(i). \quad (3.7)$$

Thus, the edge states are modified in the presence of a magnetic field. The condition of the convergence of the wave function becomes $\Delta_k \leqslant 1$, which then defines the region of the flat band. Note that Δ_k has q internal degrees of freedom. In other words, there are q solutions, which give the same value of Δ_k. For example, in the case of $\phi = 1/4$, there are four wave numbers, which give $\Delta_k = 0$, i.e, $k = \pm 3/4\pi$, $\pm 1/4\pi$, the charge density corresponding to each wave number is depicted in Fig. 10. The charge density does not penetrate to the inner sites farther than up to the $(4+1)$-th zigzag chain, and there are four kinds of localized modes corresponding to the four internal degrees of freedom of Δ_k. Thus, the edge states in a magnetic field behave as the zero-field edge states with q internal degrees of freedom.

Next, we discuss the DOS of the edge state in the absence of a magnetic field, which will be used in the calculation of the Pauli susceptibility of zigzag ribbons in the later section. As we have seen in this section, the edge state penetrate to inner sites when the wave number changes from π to $2/3\pi$. If we consider the graphite ribbons with width N, two edge states, which come from both sides of the edge, will overlap with each other and develop the bonding and antibonding configurations. Since the magnitude of the overlap becomes

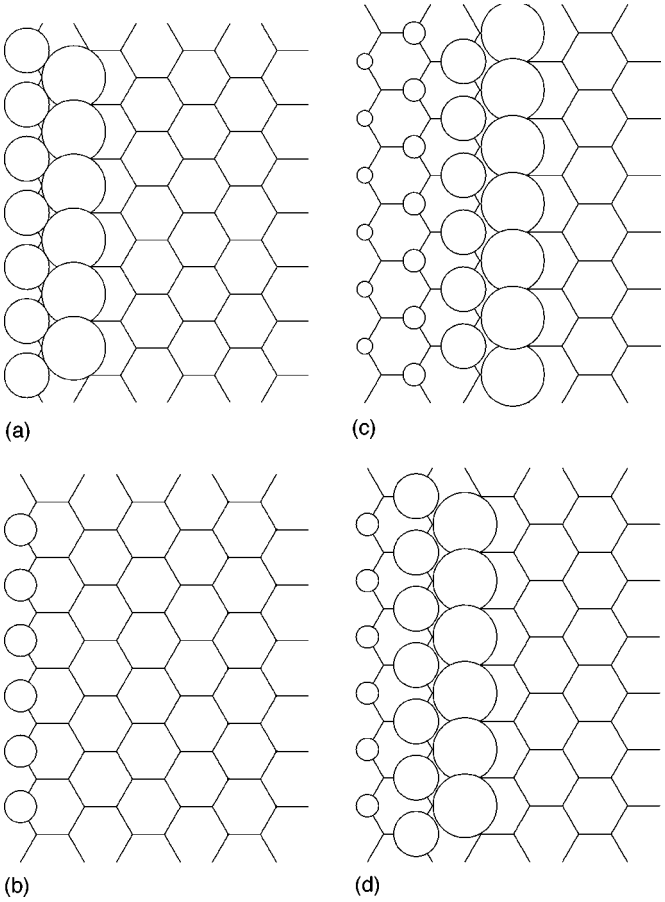

FIG. 10. The charge density of the edge state at (a) $k=-3/4\pi$, (b) $k=-1/4\pi$, (c) $k=1/4\pi$, and (d) $k=3/4\pi$, where the radius of the circle denotes the magnitude of the charge density.

larger when the wave number approaches $2/3\pi$, the band gap between the bonding and antibonding state formed by the two edge states gets larger toward $k=2/3\pi$. Therefore, the partly flat bands have a slight dispersion, which depends on the ribbon width N. In order to calculate the DOS, we first have to derive the precise energy dispersion for the edge states. The energy dispersion is calculated by the overlapping of two edge states. From Eq. (3.3), the amplitude of the edge state, which penetrates from the first zigzag line, is given by

$$\Psi_n = D_k^{n-1} \equiv \Psi_A, \tag{3.8}$$

which is located only on the A sublattice. On the other hand, the amplitude of the edge state, which penetrates from the Nth zigzag line, is given by

$$\Psi_{N-n} = D_k^{n-1} \equiv \Psi_B, \tag{3.9}$$

which is located only on the B sublattice. By using the tight-binding Hamiltonian, the overlapping of two edge states is easily calculated,

$$\langle \Psi_A | H | \Psi_B \rangle = N D_k^{N-1}(-2t - tD_k) = T_k, \tag{3.10}$$

where $D_k = -2\cos(k/2)$. Therefore, the energy spectrum of the edge states is given by the following eigenvalue problem:

$$\begin{pmatrix} 0 & T_k \\ T_k & 0 \end{pmatrix} \begin{pmatrix} C_1 \\ C_2 \end{pmatrix} = \epsilon_k \begin{pmatrix} C_1 \\ C_2 \end{pmatrix}. \tag{3.11}$$

By diagonalization of this Hamiltonian matrix, we find the energy spectrum

$$E_k = -2tND_k^{N-1}\left[-2t + 2t\cos\left(\frac{k}{2}\right)\right]. \tag{3.12}$$

From this equation, around $k=\pi$, the spectrum is given by $E \sim k^N$.

Therefore, the DOS related to the edge states has the form,

$$\rho(\epsilon) = \frac{\partial k}{\partial \epsilon} \sim \frac{1}{N}\epsilon^{\alpha}, \tag{3.13}$$

where $\alpha = 1/N - 1$. Note that this DOS has a power-law dependence, which is different from the ordinary van Hove singularity of $\rho \sim 1/\sqrt{E}$ observed in the one-dimensional system. It is also found that the renormalized DOS is inversely proportional to the ribbon width, which has been already confirmed by numerical calculation.[2]

IV. ORBITAL DIAMAGNETISM OF GRAPHITE RIBBONS

It is well known that graphite shows a large anisotropic diamagnetic susceptibility, while aromatic molecules show only weak diamagnetism. This fact tells us that the orbital diamagnetic susceptibility is sensitive to the size of graphite fragments. Therefore, we would like to clarify the size and edge shape effect on the orbital susceptibility, in order to understand the magnetic properties of nanographite ribbons. Similar calculations of the orbital diamagnetic susceptibility on carbon nanotubes have been done by several authors.[11,12] They found that there are universal scaling rules in the orbital susceptibility as a function of the Fermi energy, the temperature, and the size of the nanotubes. Since it is also expected that graphite ribbons have such scaling rules, we study the scaling properties of the orbital susceptibility and the dependence on the edge shape.

In this section, the orbital diamagnetic susceptibility χ_{orb} of graphite ribbons is calculated in terms of the 2nd derivative of the free energy $F(H,T)$ with respect to the magnetic field. The free energy is given by

$$F(H,T) = \mu N - \frac{1}{\beta\pi}\int_{BZ} dk \sum_n ln\{1 + e^{-\beta[\epsilon_{k,n}(H)-\mu]}\}, \tag{4.1}$$

where $\beta = 1/k_B T$ and μ is the chemical potential and $\epsilon_{k,n}(H)$ (n is the band index) is the energy spectrum of the graphite ribbons in the magnetic field, as calculated in the previous section. Then the magnetic moment $M(H)$ and magnetic susceptibility $\chi(H)$ per site for finite temperature and arbitrary magnetic field H become

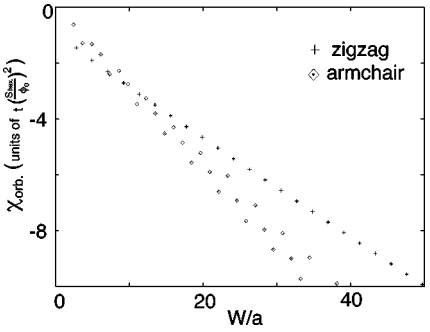

FIG. 11. The ribbon width dependence of the orbital diamagnetic susceptibility χ_{orb} of graphite ribbons at $T=0$.

$$M(H)=-\frac{1}{N_e}\frac{\partial F}{\partial H}=-\frac{1}{N_e\pi}\int dk\sum_n \frac{1}{e^{\beta(\epsilon_{k,n}-\mu)}+1}\frac{\partial \epsilon_{k,n}}{\partial H}, \tag{4.2}$$

and

$$\chi(H)=\frac{1}{N_e}\frac{\partial M}{\partial H}$$
$$=-\frac{1}{N_e\pi}\int dk\sum_n \left\{ -\frac{\beta}{4\cosh^2\frac{\beta(\epsilon_{k,n}-\mu)}{2}}\left(\frac{\partial \epsilon_{k,n}}{\partial H}\right)^2 + \frac{1}{e^{\beta(\epsilon_{k,n}-\mu)}+1}\frac{\partial^2\epsilon_{k,n}}{\partial H^2}\right\}. \tag{4.3}$$

The zero-field magnetic susceptibility $\chi_0(T)$ for finite temperature is given by

$$\chi(T)=-\frac{1}{N_e\pi}\left(\frac{S}{\phi_0}\right)^2\int \mathrm{d}k\sum_n^{occ.}\frac{1}{\mathrm{e}^{\beta(\epsilon_{k,n}-\mu)}+1}\left(\frac{\partial^2\epsilon_{k,n}}{\partial H^2}\right), \tag{4.4}$$

where S is the area of a hexagonal ring. N_e is the electron number in the system.

The width dependence of the orbital susceptibility χ_{orb} at $T=0$ is shown in Fig. 11. Analogous to the graphite sheets, the aromatic molecules or the carbon nanotubes, the graphite ribbons exhibit diamagnetism. The magnitude of $\chi_{orb}(T\approx 0)$ grows linearly with increasing W in accordance with the fact that χ_{orb} of the graphite sheet diverges in the zero-temperature limit. A remarkable point is the different slope in the W dependence of χ_{orb} for armchair and zigzag ribbons. Actually, the difference between the susceptibilities of the two types of ribbons increases for larger W. At a first glance, this result may seem unphysical, because one might attribute the difference to an edge effect, which should diminish for wider ribbons. The origin of this discrepancy, however, is based on topological properties as we will show shortly. We would like also to mention the aspect that χ_{orb} for the armchair ribbons shows some oscillations as a function of W. This is due to the fact that armchair ribbons are metallic or insulating depending on W. On the other hand, no oscillations occur for zigzag ribbons, as they are metallic for all W.

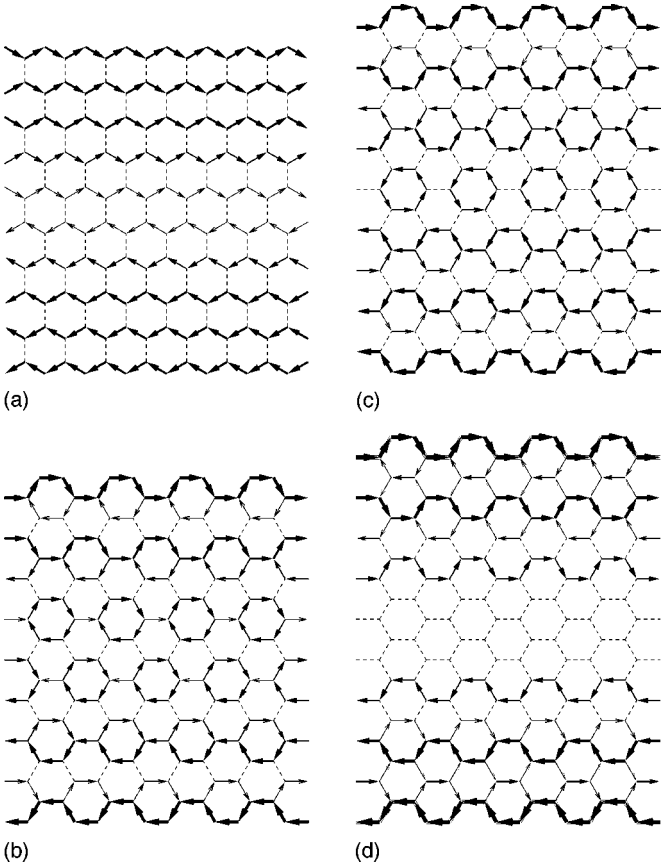

FIG. 12. The texture of the ring currents for (a) zigzag ribbon ($N=10$) and armchair ribbons of (b) $N=18$, (c) $N=19$, and (d) $N=20$. In zigzag ribbon, because of the symmetry of the lattice, the ring currents along the vertical bonds are zero. In armchair ribbons of $N=18$ and 19, the Kekulé pattern is clear.

The difference of the slope in χ_{orb} and M_{orb} is related to the more microscopic and configurational aspect of the ribbons. An important point to take into account is the ring current susceptibility in the equilibrium state, because the magnetic moments and ring currents are related in the following way

$$M=\frac{1}{c}\int \mathrm{d}\boldsymbol{V}\boldsymbol{r}\times\boldsymbol{j}, \tag{4.5}$$

where $\boldsymbol{r}$ is the position and $\boldsymbol{j}$ is the current operator.[17] $\int \mathrm{d}\boldsymbol{V}$ means volume integral. The current $\boldsymbol{j}$ is described on each bond (i,j) by

$$J_{ij}=\mathrm{i}\frac{et}{\hbar}(\mathrm{e}^{\mathrm{i}2\pi\phi_{ij}}c_i^\dagger c_j-\mathrm{H.c.}) \tag{4.6}$$

The ring currents also contribute to the linear response for weak magnetic fields. It is straightforward to calculate them and the corresponding susceptibility. The pattern of the ring currents for (a) a zigzag ribbon of $N=10$, and armchair ribbons of (b) $N=18$, (c) $N=19$, and (d) $N=20$ are shown in Figs. 12(a)–12(d), respectively. The magnitude [in the units

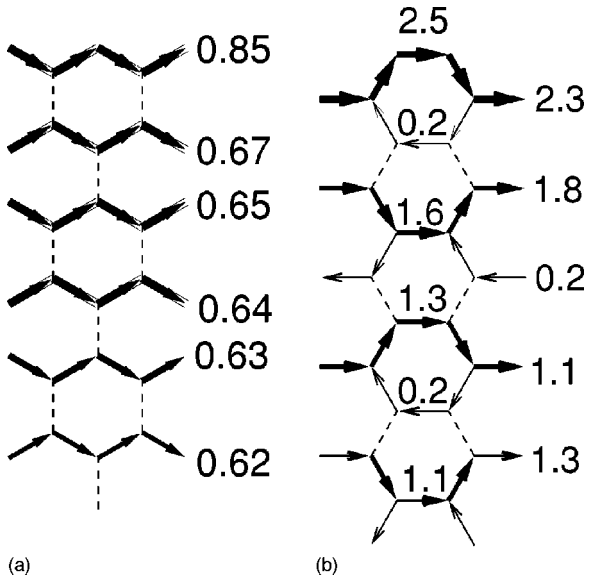

FIG. 13. Current flow and magnitude near the edge for (a) zigzag ribbon ($N=50$) and armchair ribbon ($N=50$).

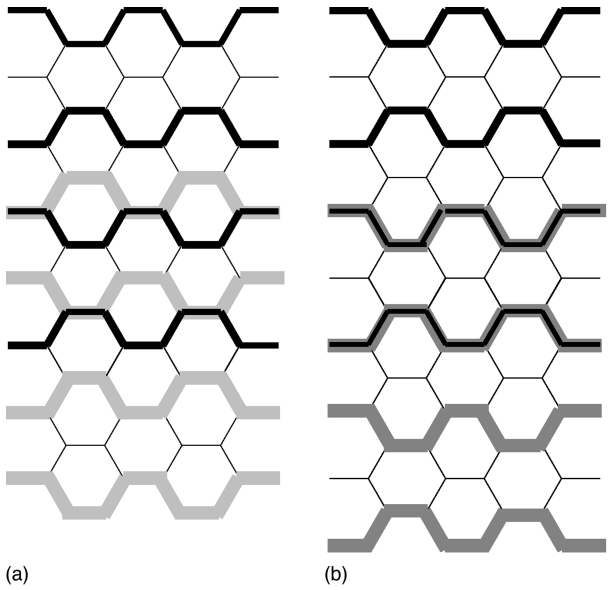

FIG. 14. Schematic picture of ring-current flow generated by the interference.

of $J_0(=et/\hbar)$] and directions of the ring current near the graphite edge is further given in detail in Fig 13. We can easily find that the current flow is symmetric with respect to $x=0$ and the total current in the y direction vanishes, because we consider an equilibrium state. The pattern of the current flow is strikingly different for the zigzag and the armchair ribbons. In zigzag ribbons, due to the lattice symmetry, the currents along the vertical bonds are exactly zero. The currents flow only along the horizontal bonds, whose directions are antisymmetric with respect to $x=0$. For armchair ribbons, the current distribution is quite different, because currents flow also on vertically oriented bonds, and exhibit a clear Kekulé-type of pattern. Note that the Kekulé pattern is more pronounced when $N\neq 3M-1$ ($M=1,2,3,\cdots$), which corresponds to the semiconducting armchair ribbon, whereas it is less distinct for the metallic case, $N=3M-1(M=1,2,3,\cdots)$, where almost no currents are found close to the ribbon center. The reason can be attributed to the interference effect between the current flows assosiated with the two edges. As shown in Fig. 13(b), the currents are stronger along the cispolyacetylene, which is separated by one dimer lines. For $N\neq 3M-1$ and $N=3M-1$, the ring current patterns are depicted schematically in Figs. 14(a) and 14(b), where thick bold lines denote dominant right-going currents while thick shaded lines are for the left-going currents. It is easy to find that for $N\neq 3M-1$ both types of lines tend to avoid each other and form a Kekulé pattern around the center of the ribbons. However, when $N=3M-1$, the lines lie perfectly on top of each other so that the left- and right-going currents cancel each other around the center of ribbon. Thus, the effect of the lattice topology near graphite edge drastically changes the ring current flow in the whole sample.

In Fig. 15, the magnitude of the ring-current susceptibility J is plotted as a function of x/W with a fixed position y for (a) zigzag ribbons, (b) armchair ribbons with ($N\neq 3M-1$), and (c) armchair ribbons with ($N=3M-1$). Interestingly, each graphite ribbon has a scaling behavior as a function of x/W and the magnitude of the ring currents has a power-law decay. These facts further emphasize that the edge-shape effect is significant in nanographites.

Next we show the Fermi energy dependence of χ_{orb}. Actually in real graphite materials, a small change in the carrier density from the half filling is possible and can even be controlled by substrate properties. The calculated Fermi energy dependence is shown in Fig. 16, where it is found that χ_{orb}/W is a universal function of μW. We normalize χ_{orb} by dividing it by W, since it is proportional to W (Fig. 11). Furthermore, we multiply E_F by W, because the direct gap at $k=0$ is proportional to the $1/W$ at $k=0$ for armchair ribbons and at $k=2\pi/3$ for zigzag ribbons as is demonstrated in the Appendix.

As a final point in this section, we show the temperature dependence of χ_{orb} in Fig. 17, which is important from the viewpoint of experiments on nanographites. In all cases the magnitude of χ_{orb} decreases with increasing temperature. It is also found that the temperature dependence of χ_{orb}/W scales as a function of βW, because the energy gap is proportional to the $1/W$. Our calculation also demonstrates that the edge effect becomes more significant with lower temperature.

V. PAULI PARAMAGNETISM OF GRAPHITE RIBBONS

In the previous section, we have seen that the orbital diamagnetic susceptibility depends on the edge shape in nanographite ribbons, especially, the topology of the lattice strongly affects the flow of diamagnetic ring currents. Here we discuss another important component of the magnetic susceptibility, Pauli paramagnetic susceptibility χ_P, because zigzag ribbons have a sharp peak of DOS at the Fermi level. The width of the peak of DOS at the Fermi level has the order of meV, which is comparable to the temperature scale of room temperature. Therefore, it is expected that the Pauli susceptibility of zigzag ribbons might be sensitive to temperature, although the Pauli susceptibility of other usual metals is temperature independent. On the other hand, since the

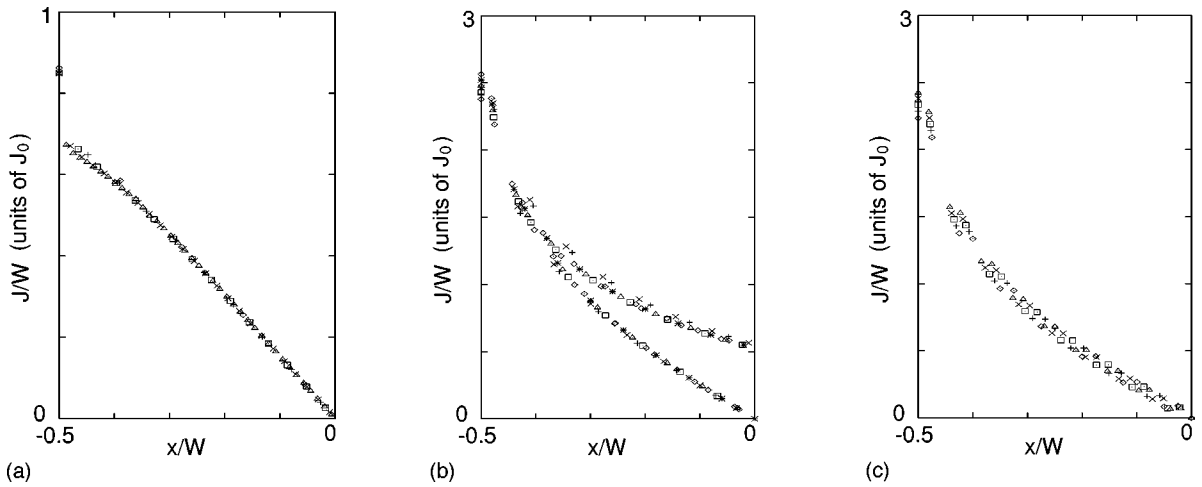

FIG. 15. The position dependence of magnitude of the ring currents for (a) zigzag ribbons, (b) armchair ribbons ($N \neq 3M-1$), and (c) armchair ribbons ($N=3M-1$).

DOS of armchair ribbons at $\epsilon=0$ is zero or very tiny, we can neglect the effect of the Pauli paramagnetism in armchair ribbons.

The magnetic moment by the Zeeman effect is

$$M=\mu_B(n_\uparrow-n_\downarrow), \tag{5.1}$$

where μ_B is Bohr magneton and $n_\uparrow(n_\downarrow)$ means the electron density with up-spin (down-spin). The electron density at arbitrary temperature for each spin is given by

$$n_\sigma=\frac{1}{\pi}\int_{1st\mathbf{BZ}} \mathrm{d}k \sum_n \frac{1}{1+\mathrm{e}^{\beta(\epsilon_{n,k}-\sigma\mu_B H)}}, \tag{5.2}$$

where $\sigma(=\uparrow,\downarrow)$ means spin index. Therefore, the Pauli susceptibility χ_P per site is given by

$$\chi_P=\lim_{T\to 0}\frac{\partial M}{\partial H}=\frac{\beta\mu_B^2}{\pi N_e}\sum_n \int \mathrm{d}k \frac{1}{\cosh(\beta\epsilon_{n,k})}, \tag{5.3}$$

where $\beta=1/k_BT$. Room temperature ($T\sim 300$ K) corresponds to $\beta\sim 0.25$. We numerically calculated the finite temperature Pauli susceptibility of graphite ribbons using this equation up to room temperature.

It is possible to clarify the contribution of the edge states to χ_P. As we have seen in Sec. III, the DOS due to the edge states is given by Eq. (3.13). After the substitution of Eq. (3.13) into Eq. (5.3), we replace the k integration by the energy integration. Then we can obtain the χ_P contribution due to the edge states as,

$$\chi_P=\frac{1}{N_e N\beta^\alpha}\int \mathrm{d}x \frac{x^\alpha}{\cosh x+1}\sim\frac{1}{N}T^\alpha, \tag{5.4}$$

where x is $\beta\epsilon_k$ and α is $1/N-1$. Interestingly, χ_P has the Curie-like temperature dependence, although in normal metals χ_P is basically constant in the temperature. The exponent of χ_P depends on the ribbon width through α. When N becomes infinite, the exponent α approches -1 and χ_P show the Curie-law. However, in this limit, the contribution of χ_P is diminished by a factor $1/N$ in Eq. (5.4).

Numerical results of the Pauli susceptibility χ_P of zigzag ribbons up to room temperature are shown in Fig. 18 for various values of N. As expected, because of the edge states, χ_P shows Curie-like temperature dependence. In the inset of Fig. 18, we plotted the N dependence of α, which was calculated by the least-square method and has a good agreement with the line of $1/N-1$.

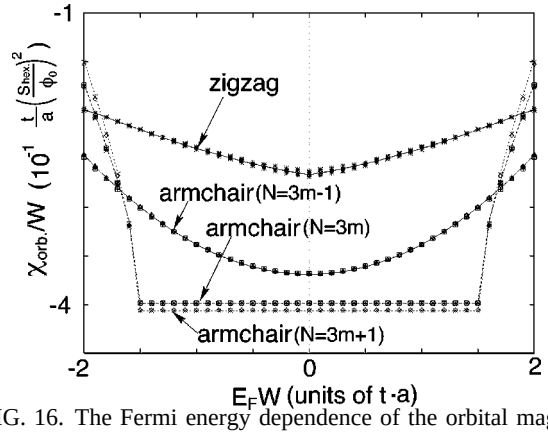

FIG. 16. The Fermi energy dependence of the orbital magnetic moments χ_{orb} of graphite ribbons at $T=0$.

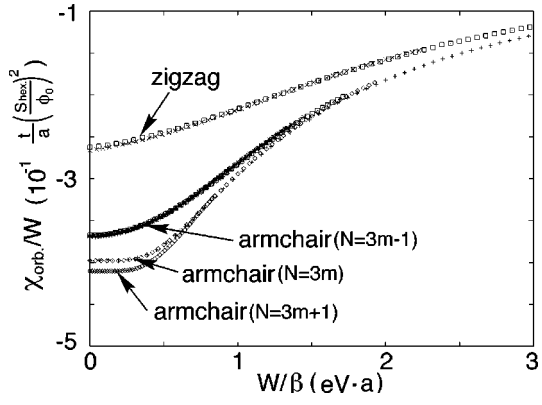

FIG. 17. The temperature dependence of χ_{orb}, where χ_{orb} is scaled by $1/W$ and β is scaled by W.

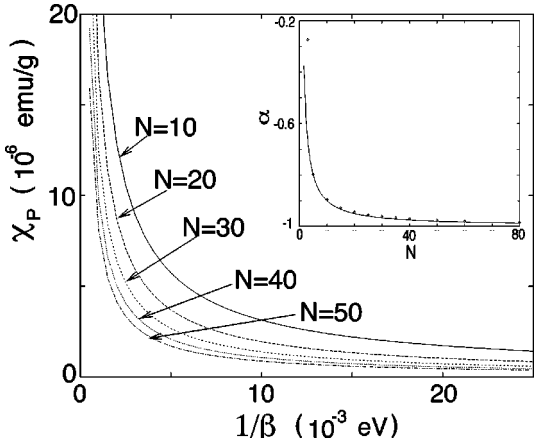

FIG. 18. The temperature dependence of χ_P for $N=10,20,\ldots,50$ up to room temperature. In the inset, the exponet is plotted on the width N and show a good agreement with the line of $1/N-1$.

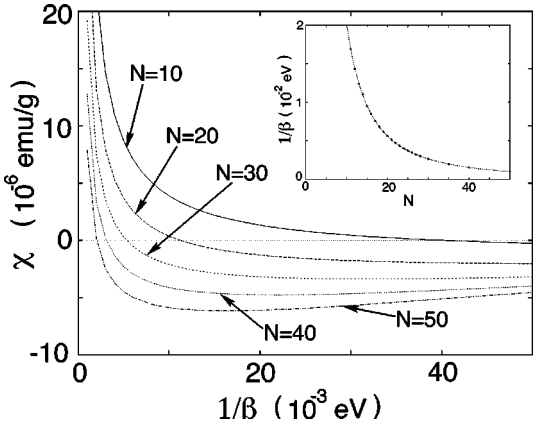

FIG. 19. The temperature dependence of total susceptibility χ, which is $\chi_{orb}+\chi_P$ is shown for $N=10,20,\ldots,50$. In the inset, the width dependence of crossing temperature, where $\chi=0$.

The observed susceptibility χ is essentially the sum of the orbital χ_{orb} and the Pauli susceptibility χ_P. The temperature dependence of the total susceptibility χ is shown in Fig. 19. The total susceptibility χ shows the diamagnetic behavior in the high-temperature regime and paramagnetic behavior in the low temperature. In the inset, the width dependence of the crossing temperature, i.e., $\chi=0$, is plotted, which is well fitted by $1/\beta=10^{0.1526}\times N^{-1.846}$.

Here we should remind you that both aromatic molecules and bulk graphite show diamagnetic behavior, however, nanographite with zigzag edges have a remarkable paramagnetic behavior because of the edge state. If this paramagnetic behavior is experimentally detected, it will be an indirect evidence of the existence of the edge state.

VI. SUMMARY AND DISCUSSION

In this manuscript, we discussed the electronic and magnetic properties of nanographite in magnetic field, by using the single orbital tight binding model with Peierls phase. Deriving the Harper equation for the graphite lattice, we studied the energy spectrum and dispersion in a magnetic field. At $\phi=0$, it is found that zigzag ribbons have partly flat bands at the Fermi level, which is attributed to the edge localized states having nonbonding character. In terms of the Harper equation, the edge state can be analytically described even in the presence of a magnetic field. We also studied orbital diamagnetic properties of the nanographite ribbons, where we found that the diamagnetic susceptibility χ_{orb} is very sensitive to the size and edge shapes of graphite ribbons. It is emphasized that the flow of the orbital diamagnetic ring currents significantly depend on the lattice topology near the graphite edges. Especially, in the case of armchair ribbons, the pattern of the ring currents has drastically changed because of the interference effect of two edges. It is also found that the orbital diamagnetic susceptibility χ_{orb} is scaled as a function of the temperature, Fermi energy, and ribbon width. Because the edge states induce a sharp peak of DOS at the Fermi level, the Pauli paramagnetic susceptibility should be an important component in nanographite with zigzag edges. Therefore, in the last section the Pauli susceptibility in zigzag ribbons has been studied, where we found that the zigzag ribbons with nanometer size show the Curie-like temperature dependence of the Pauli susceptiblity in contrast to usual metals. From this significant contribution of the Pauli susceptibility, it is found that the observed susceptibility $\chi(=\chi_P+\chi_{orb})$ of zigzag ribbons show diamagnetic behavior at high temperature and paramagnetic behavior at low temperature.

Here we introduce an interesting experimental result, which might be connected with our theoretical results. Some graphite-related materials consisting of nanographites, e.g., activated carbon fibers (ACF), amorphous carbons, carbon blacks, defective carbon nanotubes, etc., show actually anomalous behaviors in the magnetic susceptibility. While bulk graphite has a large diamagnetic and anisotropic susceptibility, a certain type of ACF with a huge specific surface area up to $3000m^2/g$ (believed to consist of an assembly of minute graphite fragments with a dimension of 20×20 Å) exhibits a paramagnetic response at room temperature and a strong Curie-like behavior in low temperature.[18] This kind of anomalous behavior of the susceptibility is also observed in many amorphous carbons and defective carpet-rolled carbon nanotubes.[19] Although zigzag and armchair edges coexist in real carbon material, this behavior of magnetic susceptibility is consistent with our results. Although the sample production of graphite-related materials has still insufficient influence on size and edge shapes, recently there are some experimental attempts to synthesize and nanographite systems and to control the size and edge shapes. One is ''graphitization'' of diamond powder with grain sizes $40-50$ Å. Another method to produce nanographites is epitaxial growth on substrates with step edges.[20] Therefore, we expect that in the near future the magnetic properties of nanographites will be observable so that the influence of the edge states on magnetic properties can be tested in a controlled way.

ACKNOWLEDGMENTS

The authors are grateful to K. Kusakabe, H. Tsunetsugu, K. Nakada, and M. Igami for many helpful discussions. K.W. acknowledges the financial support of the Japan Society for the Promotion of Science for Young Scientists. This paper has been supported by a Grant-in-Aid for Scientific

Research (09875066) 1997 and by a Grant-in-Aid for Scientific Research on Priority Areas ''Carbon Alloys'' (09243105) from the Ministry of Education, Science and Culture, Japan (M.F.).

APPENDIX: ENERGY GAP

In this appendix, we analytically show that both the direct gap Δ_a at $k=0$ of sufficiently wide armchair ribbons and the direct gap Δ_z at $k=2\pi/3$ of sufficiently wide zigzag ribbons are inversely proportional to the width of graphite ribbon W. This result supports that the χ_{orb}/W is scaled as a function of the μW (μ is chemical potential).

First, we examine the energy gap Δ_a at $k=0$ of armchair ribbons. It is easy to find that at the $k=0$ the Hamiltonian can be rewritten as

$$H=-t\sum_{j=1}^{N}\left[\sum_{\mu=1}^{2}(a_{j,\mu}^{\dagger}a_{j+1,\mu}+\text{H.c.})+a_{j,1}^{\dagger}a_{j,2}+\text{H.c.}\right], \tag{A1}$$

which is equivalent to the tight-binding model for the two-leg ladder lattice having N rungs.[1] The site indices $(j,1)$ and $(j,2)$ correspond to the $jA(B)$ and $jB(A)$ sites, respectively, when j is even(odd). The eigenvalues are evaluated as $\epsilon^{\pm}=-2t\cos n\pi/(N+1)\pm t$ $(n=1,2,\ldots,N)$. It should be noted that the system is metallic only when $N=3m-1$, because ϵ^{+} and ϵ^{-} become zero for $n=m$ and $2m$, respectively. Therefore, Δ_a are 0 for $N=3m-1,2(2t\cos\{[m/(3m+1)]\pi\}-t)$ for $N=3m$ and $(2t\cos\{[(m+1)/(3m+1)]\pi\}-t)$ for $N=3m+1$, respectively. After the elimination of N in terms of $W=(N-3)\sqrt{3}/2+\sqrt{3}$ and the Taylor expansion under the condition of $1/W\ll 1$, we can obtain the following results

$$\Delta_a\sim\begin{cases}0 & N=3M-1\\ \dfrac{\pi}{W+\dfrac{\sqrt{3}}{2}} & N=3M\\ \dfrac{\pi}{W} & N=3M+1.\end{cases} \tag{A2}$$

Thus, the Δ_a is inversely proportional to the ribbon width.

Similarly, we can obtain the energy gap Δ_z at $k=2\pi/3$ of zigzag ribbons. The Hamiltonian of zigzag ribbons at $k=2\pi/3$ is rewritten as

$$H=-t\sum_{i=1}^{2N}(a_i^{\dagger}a_{i+1}+\text{H.c.}), \tag{A3}$$

which is equivalent to the tight binding model for the one-dimensional lattice having $2N$ sites. The site index i corresponds to iA, if i is an odd number, and to iB, if i is an even number. The eigenvalues are evaluated as $\epsilon=-2t\cos n\pi/(2N+1)$ $(n=1,2,\ldots,N)$. Therefore, Δ_z is $4(2t\cos\{[(N+1)/(2N+1)]\pi\})$. After the elimination of N in terms of $W=\sqrt{3N}/2-1$ and Taylor expansion under the condition of $1/W\ll 1$, we can obtain the following results.

$$\Delta_z\sim\frac{\pi}{W}. \tag{A4}$$

Thus, the Δ_a is also inversely proportional to the ribbon width.

*Deceased.

[1] M. Fujita, K. Wakabayashi, K. Nakada, and K. Kusakabe, J. Phys. Soc. Jpn. **65**, 1920 (1996).

[2] K. Nakada, M. Fujita, G. Dresselhaus, and M.S. Dresselhaus, Phys. Rev. B **54**, 17 954 (1996).

[3] M. Fujita, M. Igami, and K. Nakada, J. Phys. Soc. Jpn. **66**, 1864 (1997).

[4] K. Wakabayashi, M. Sigrist, and M. Fujita, J. Phys. Soc. Jpn. **67**, 2089 (1998).

[5] K. Nakada, M. Igami, and M. Fujita, J. Phys. Soc. Jpn. **67**, 2388 (1998).

[6] Y. Miyamoto, K. Nakada, and M. Fujita, Phys. Rev. B (to be published).

[7] P.R. Wallace, Phys. Rev. **71**, 622 (1947).

[8] R. Saito, M. Fujita, G. Dresselhaus, and M.S. Dresselhaus, Appl. Phys. Lett. **60**, 2204 (1992); R. Saito, M. Fujita, G. Dresselhaus, and M.S. Dresselhaus, Phys. Rev. B **46**, 1804 (1992).

[9] F. London, J. Phys. Radium **8**, 397 (1937).

[10] A.H. MacDonald, Phys. Rev. B **29**, 6563 (1984).

[11] H. Ajiki and T. Ando, J. Phys. Soc. Jpn. **62**, 1255 (1993).

[12] J.P. Lu, Phys. Rev. Lett. **74**, 1123 (1995).

[13] D.R. Hosfstadter, Phys. Rev. B **14**, 2239 (1976).

[14] Y. Hatsugai, Phys. Rev. B **48**, 11 851 (1993).

[15] R. Rammal, J. Phys. (Paris) **46**, 1345 (1985).

[16] R. Rammal, G. Toulouse, M.T. Jaekel, and B.I. Halperin, Phys. Rev. B **27**, 5142 (1983).

[17] R.M. White, *Quantum Theory of Magnetism* (Springer-Verlag, Berlin, 1983).

[18] A. Nakayama, K. Suzuki, T. Enoki, S.L. di Vittorio, M.S. Dresselhaus, K. Koga, M. Endo, and N. Shindo, Synth. Met. **55-57**, 3736 (1993); A. Nakayama, Ph.D thesis, Department of Chemistry, Tokyo Institute of Technology, 1996.

[19] S. Bandow, J. Appl. Phys. **80**, 1020 (1996).

[20] M. Terai, N. Hasegawa, M. Okuzawa, S. Otani, and C. Oshima, Appl. Surf. Sci. **130-132**, 876 (1998); N. Hasegawa, M. Terai, M. Okuzawa, C. Oshima, and S. Otani (unpublished).